

Presented at the Conference on Acoustic Emissions by the Acoustical Society of America and the Acoustical Society of Japan, Honolulu, Hawaii, November 27-December 1, 1978

LBL-8335 e.2

ACOUSTIC EMISSION SOURCES
IN BRITTLE SOLIDS

RECEIVED
LAWRENCE
BERKLEY LABORATORY

A. G. Evans

FEB 26 1979

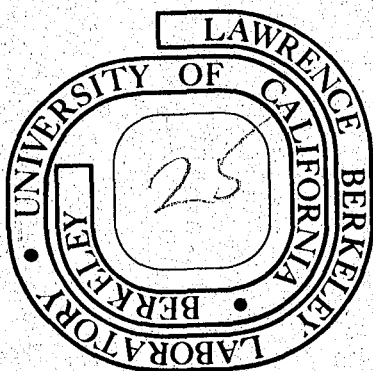
October 1978

LIBRARY AND
DOCUMENTS SECTION

Prepared for the U. S. Department of Energy
under Contract W-7405-ENG-48

TWO-WEEK LOAN COPY

This is a Library Circulating Copy
which may be borrowed for two weeks.
For a personal retention copy, call
Tech. Info. Division, Ext. 6782



LBL-8335 e.2

LEGAL NOTICE

This report was prepared as an account of work sponsored by the United States Government. Neither the United States nor the Department of Energy, nor any of their employees, nor any of their contractors, subcontractors, or their employees, makes any warranty, express or implied, or assumes any legal liability or responsibility for the accuracy, completeness or usefulness of any information, apparatus, product or process disclosed, or represents that its use would not infringe privately owned rights.

ACOUSTIC EMISSION SOURCES IN BRITTLE SOLIDS

A. G. Evans

Materials and Molecular Research Division, Lawrence Berkeley Laboratory
and Department of Materials Science and Engineering,
University of California, Berkeley, California 94720

ABSTRACT

The sources of acoustic emission that are prevalent in brittle solids are examined, especially microcrack sources and sources that accompany macrocrack extension. The emission amplitude distributions are derived using crack opening displacement solutions pertinent to each source type, and assuming an extreme value size distribution of precursors consistent both with the functional form of typical emission amplitude distributions and with defect size observations. Acoustic emission event rates are derived from the stress and time dependence of crack growth. Stress history effects are afforded particular emphasis. Finally, some applications of acoustic emission that emerge from the analysis of the source characteristics are briefly evaluated.

I. INTRODUCTION

Brittle solids are often profuse sources of acoustic emission. The acoustic emission derives from microfracturing events that occur prior to ultimate failure. Microfracture typically involves time independent and time dependent components; whose coupling leads to several interesting functional relations between the acoustic emission and the stress history. Such stress history phenomena are an important theme of this paper. The intensity of acoustic emission from brittle solids exhibits a strong dependence on microstructure. The role of microstructure is thus a second primary theme. Acoustic emission can, in certain situations, be used as a technique for predicting failure. The circumstances which permit effective failure prediction are examined in the final section of the paper.

The discussion of acoustic emission will emphasize the event amplitudes and the event rates; no specific attention will be devoted to the frequency characteristics. The amplitudes will be represented by distribution functions that can be related to the characteristics of the source and the extrinsic variables. The event rates will be related (in particular) to the stress history, and the imminence of final failure.

It is convenient to consider two sources of acoustic emission. The first derives from the formation of isolated microcracks, either at grain boundaries or at second phase particles (or inclusions). The second emanates from the incremental extension of macrocracks in

polycrystalline or multi-phase materials. These sources of emission yield different amplitude distributions and event rates and are treated separately. The source distinctions discerned from this analysis will subsequently be used as a basis for considering acoustic emission as a technique for predicting failure.

II. ACOUSTIC EMISSION FROM ISOLATED MICROCRACKS

2.1 General Considerations

The amplitude σ of the stress wave emitted during the formation of a crack is related to the local displacement u_z that accompanies crack development (Fig. 1); specifically,¹

$$\sigma(r,t) = \mu \delta \int_S u_z dS \quad (1)$$

where μ is the shear modulus, S represents the crack surface and δ is a parameter that depends (through the event duration) on the frequency ω , the wave velocity c , the distance from the source r , etc.

The geometric shape of isolated cracks located at grain boundaries or inclusions will be approximated by an ellipse: with semi-major and semi-minor axes designated a and b respectively. The displacement integral $\int_S u_z dS$ can then be written explicitly as;²

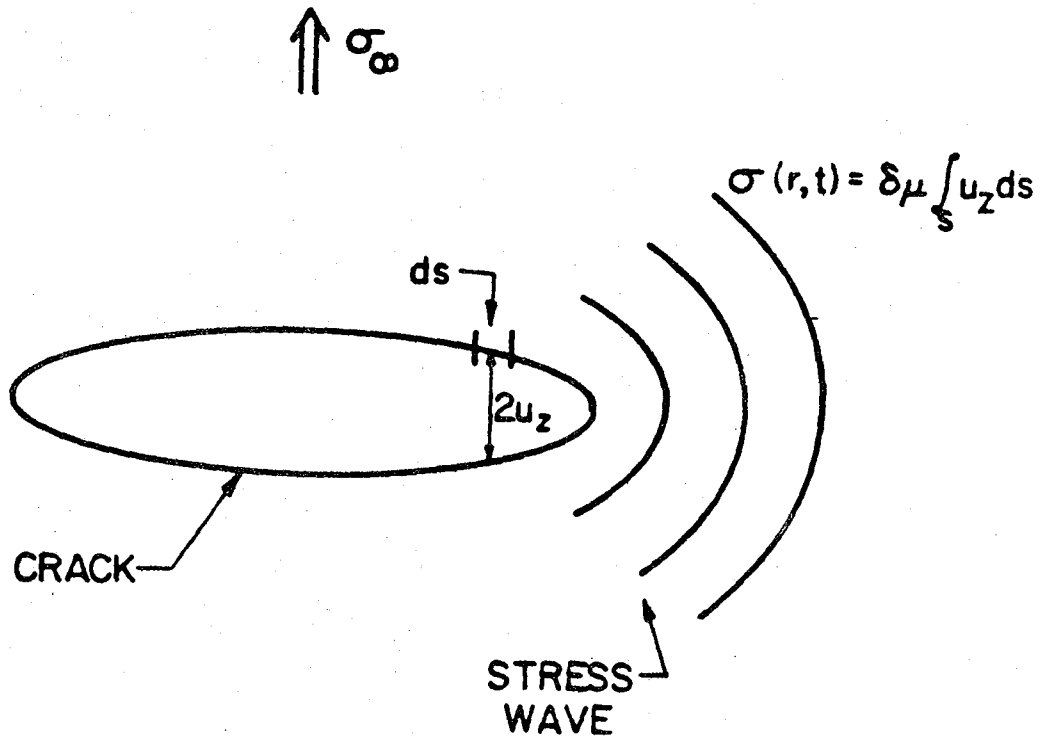
$$\int_S u_z dS = \frac{4\pi ab^2 \sigma_{zz}^1 (1-\nu)}{3\mu \epsilon(k)} \quad (2)$$

where σ_{zz}^1 is the tensile stress normal to the crack surface, ν is Poisson's ratio and $\epsilon(k)$ is the elliptic integral of the second kind (with $k^2 = 1-(b/a)^2$). The stress wave amplitude for such a crack is thus;

$$\sigma(r,t) = \left[\frac{4\pi(1-\nu)}{3 \epsilon(k)} \right] ab^2 \sigma_{zz}^1 \delta. \quad (3)$$

Therefore, the stress amplitude does not simply depend on the area A ($= \pi ab$) of the crack, but contains an additional dependence on the dimension of its minor axis b , and on the event duration parameter δ . Note that, for a crack of circular shape, radius a , the stress wave amplitude would depend on a^3 if δ were independent of the crack dimensions: this dependence has recently been inferred from experimental results obtained for inclusion fracture in steel.³

The strong dependence of the stress wave amplitude on the crack dimensions indicates that the acoustic emission amplitudes measured above the background derive primarily from the large size extreme of microcracks. One of the three extreme value functions⁴ should thus characterise the size distribution of grain boundaries (or inclusions)



XBL7811-6155

Fig. 1: A schematic indicating the relation between the crack opening and the emitted stress wave.

that afford the principal contribution to the acoustic emission amplitude. This conclusion is reinforced by the realization that the large size extreme of grain boundaries also exhibits the greatest microfracture probability⁵ (at a given level of applied stress). Recent studies suggest that the extreme value function of the second kind is an appropriate descriptor of the large extreme of grain diameters;⁶ this function has the form:

$$\Phi(d) = 1 - \exp[-(d_0/d)^k] \quad (4)$$

where $\Phi(d)$ is the probability that one (given) dimension of the grain boundary will exceed d , k is a shape parameter and d_0 is a scale parameter. Now defining an average dimension $\langle d \rangle$ of the prospective crack plane as

$$\langle d \rangle^3 = ab^2 \quad (5)$$

and noting that the stress wave amplitude is proportional to the voltage V output of the transducer,

$$V = f\sigma, \quad (6)$$

where f is the stress coefficient of the transducer, Eqs. (3), (4), (5) and (6) can be combined to yield the probability $\Phi(V)$ that the acoustic emission amplitude will exceed V (Fig. 2);

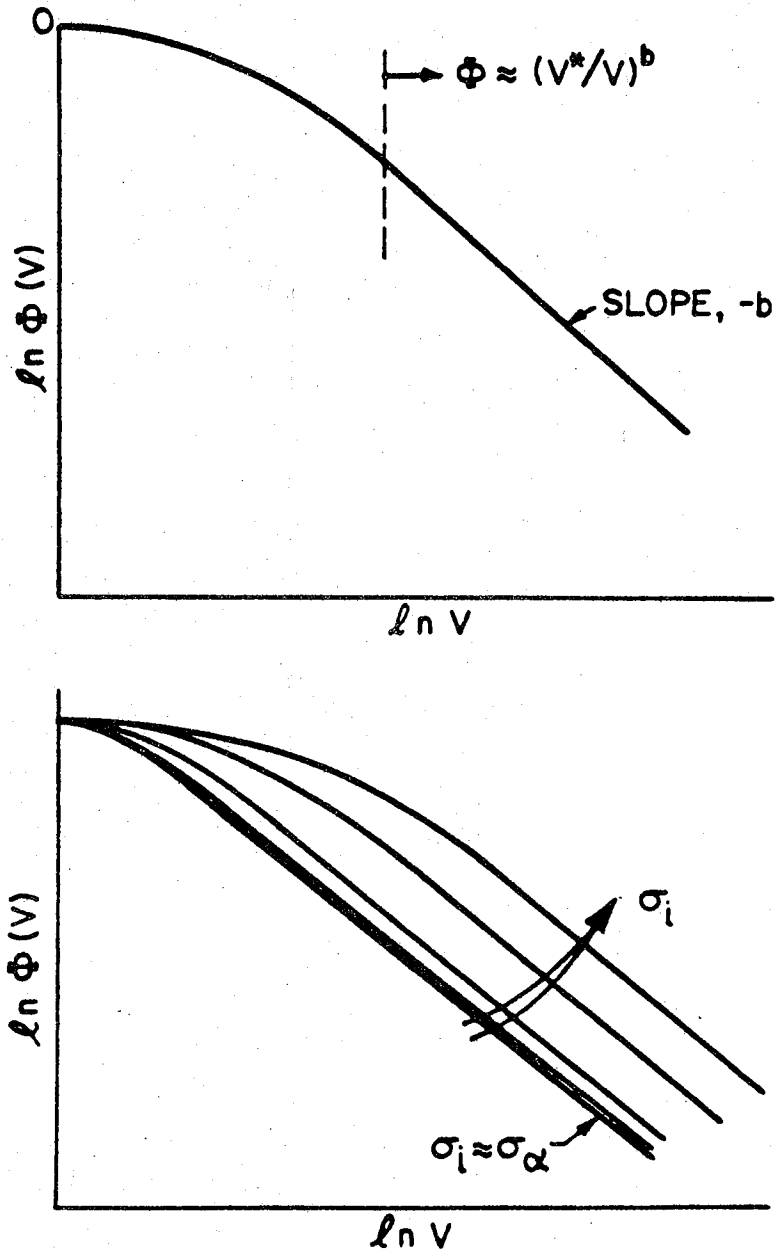
$$\begin{aligned} \Phi(V) &= 1 - \exp \left[- d_0^k \left(\frac{4\pi f(1-\nu)}{3E(k)\delta} \right)^{k/3} \left(\frac{\sigma_{zz}^i}{V} \right)^{k/3} \right] \\ &\equiv 1 - \exp \left[- \beta \left(\frac{\sigma_{zz}^i}{V} \right)^b \right]. \end{aligned} \quad (7)$$

An expression of this type has been proposed previously.⁷ Note that Eq. (7) reduces for large V (Fig. 2a) to the conventionally used (but obviously limited) expression for acoustic emission amplitudes;

$$\Phi(V) = (V^*/V)^b \quad (8)$$

where $V^* \equiv \beta^{1/b} \sigma_{zz}^i$ and $b = k/3$. Also note that Eq. (7) is not a Weibull distribution.* The specific implications of this amplitude distribution

*It is interesting, however, to appreciate that Eq. (7) does give a Weibull distribution of fracture strengths, with a shape parameter $m = 2k$ (see Eq. 12). In some instances, therefore, b and m could be related, with $b \approx m/6$. Typical values for m are the range 4-16, yielding b values between 0.7 and 2.3. Values of b are generally in this range.^{7,8,9}



XBL 7811-6160

Fig. 2: Schematics of the amplitude distribution for microcracking (a) indicating the reduced form that applies for small ϕ ; (b) the influence of the applied stress σ_i .

function depend on the detailed nature of the microcracks and therefore, the two principal modes of microcracking will be examined on a separate basis.

2.2 Grain Boundary Microcracks

The formation of stable microcracks at grain boundaries is prevalent in materials with anisotropic thermal expansion properties.⁵ In these materials stress singularities develop at grain triple points, and the stress is further intensified at small preexistent defects, (especially those located at the triple points). The stress σ_α and the stress intensity factor K are given by;⁵

$$\begin{aligned}\sigma_\alpha &= \mu\Delta\alpha\Delta T\xi(x/d) \\ K &= \mu\Delta\alpha\Delta T\sqrt{d} \kappa(x/d)\end{aligned}\quad (8)$$

when $\Delta\alpha$ is the thermal expansion anisotropy, ΔT is the temperature range over which the stress accumulates, x is the size of the triple point defect and ξ and κ are functions that depend on the grain orientations and the relative defect size. Note that K increases as the grain boundary facet dimension d increases; this provides a preference for microfracture formation at the large size extreme of the distribution of grain facets.

The total effective stress on the crack plane pertinent to the acoustic emission amplitude is the sum of the applied stress and the expansion mismatch stress. Hence,

$$\Phi(V) = 1 - \exp \left[-\beta \left(\frac{\sigma^i + \mu\Delta\alpha\Delta T \langle \xi \rangle}{V} \right)^b \right] \quad (9)$$

In materials with a relatively large thermal expansion mismatch, $\langle \sigma_\alpha \rangle \gg \sigma^i$, and thus (since $\langle \xi \rangle$ is insensitive to the grain facet size), the acoustic emission amplitude distribution will be essentially independent of the level of the applied stress. Stress independent amplitude distributions have been obtained for porcelain.⁷ Otherwise, a dependence of $\Phi(V)$ on σ^i should be anticipated (Fig. 2b).

The stress intensity factor due to the expansion mismatch is augmented by the applied stress;

$$K \approx 2\sigma^i \sqrt{x/\pi} \quad (10)$$

Superposition of K values yields a critical value for the applied stress at microfracture σ_c^i given by,

$$\sigma_c^i = \sqrt{\frac{\pi}{x}} \left[\frac{K_{gb} - \mu\Delta\alpha\Delta T\sqrt{d} \kappa(x/d)}{2} \right] \quad (11)$$

where K_{gb} is the fracture toughness of the grain boundary. The number of microfracturic events η at a stress level σ^i is thus related to the joint distributions of defect size x and grain facet length d . The appropriate relationship between these distributions has yet to be elucidated. However, reference to the solution for inclusion fracture (section 2.3) suggests the following approximate relation for time independent microfracture;

$$\eta \approx N_b \left[\frac{\sigma^i + \mu \Delta \alpha \Delta T \bar{\xi}}{\sigma_o} \right]^m A_b \quad (12)$$

where $\bar{\xi}$ is some averaged value of ξ over the defect x , m and σ_o are shape and scale parameters respectively, N_b is the total number of boundary facets subjected to the stress σ^i and A_b is the grain boundary area.

2.3 Inclusion Fracture

Inclusions in brittle materials tend to fracture from a distribution of small defects (e.g., pores) located within the inclusion and/or at the interface.¹⁰ In some cases inclusion fracture precedes final failure and yields precursor acoustic emission. But, in many other instances, inclusion fracture coincides with ultimate failure. The former situation, which is of greatest interest for present purposes, generally pertains to low toughness inclusions with an average thermal contraction coefficient comparable to that of the host material; i.e., silicon inclusions in silicon nitride.¹⁰ Inclusions with an appreciably larger thermal contraction than the host tend to generate porosity (or open cracks) by vacancy transport. The presence of the pores increases the compliance of the inclusion and thereby, limits internal stress development and the propensity for premature fracture.

The analysis of inclusion fracture is relatively straightforward. The stresses within the inclusion generated by thermal contraction mismatch and the applied stress are both uniform (at least when the inclusion shape can be approximated by an ellipsoid). The stresses can be derived using the Eshelby analysis.¹¹ The relations adopt a particularly simple form for spherical inclusions; these will be used for illustration purposes. The thermal contraction mismatch stresses are;^{11,12}

$$\sigma_\alpha = \frac{4\mu_m \Delta \alpha \Delta T}{1 + (\mu_m / \mu_i) [2(1 - 2\nu_i) / (1 - \nu_m)]} \equiv \beta * \mu_m \Delta \alpha \Delta T \quad (13)$$

where the subscripts i and m refer to the inclusion and matrix respectively. The stresses that derive from the applied stress σ^i are;¹¹

$$\sigma_{\xi} = \sigma^i \left\{ 1 + \frac{2}{3} \frac{[(\kappa_i/\kappa_m)-1](1-2\nu_m)}{(1-\nu_m)} \left(\frac{4\mu_m+3\kappa_m}{4\mu_m+3\kappa_i} \right) \right\} \equiv \zeta \sigma^i$$

where κ is the bulk modulus. Superimposing these stresses and inserting into Eq. (7) gives the acoustic emission amplitude distribution for inclusion fracture;

$$\Phi(V) = 1 - \exp \left[-\beta \left(\frac{\beta^* \mu_m \Delta\alpha \Delta T + \zeta \sigma^i}{V} \right)^b \right] \quad (15)$$

This result is similar in form to that obtained for grain boundary microfracture; however, the coefficients ($\langle \xi \rangle$, β^* , ζ) are quite different in the two cases.

The probability of inclusion fracture can be derived by specifying a strength distribution for the precursor defects within the inclusion. Specifically, the fracture probability $\Phi(\sigma)$ at a stress level σ is given for non-interacting defects by;¹⁰

$$\Phi(\sigma) = 1 - \exp - \int_{v_i}^{\sigma} dv \int_0^{\sigma} g(s) ds \quad (16)$$

where v_i is the volume of the inclusion and $g(s)ds$ is the number of defects in unit volume with a strength between s and $s+ds$. If we assume a Weibull function for $g(s)ds$, since the stress within the inclusion is uniform, Eq. (16) can be combined with Eqs. (13) and (14) to give the fracture probability for time independent fracture,

$$\Phi(\sigma) = 1 - \exp \left[- v_i \left(\frac{\beta^* \mu_m \Delta\alpha \Delta T + \zeta \sigma^i}{\sigma_o} \right)^m \right] \quad (17)$$

The number of inclusion fracture events at a uniform applied stress level σ^i for a sample containing N_i inclusions is thus;

$$\eta = (N_i - \eta + 1) \left\{ 1 - \exp \left[- \left(\frac{\beta^* \mu_m \Delta\alpha \Delta T + \zeta \sigma^i}{\sigma_o} \right)^m \sum_1^{N_i - \eta + 1} v_i \right] \right\} \quad (18)$$

which, for $\eta \ll N_i$, becomes;

$$\eta \approx N_i \left[\frac{\beta^* \xi_m \Delta\alpha \Delta T + \zeta \sigma^i}{\sigma_o} \right]^m \sum_1^{N_i} v_i \quad (19)$$

Note the direct dependence of the number of events on the inclusion volume; also, note that some fractures occur at zero stress (due to the thermal mismatch stress σ_α), such that significant additional fractures are not initiated by the applied stress until σ_ξ becomes an appreciable fraction of σ_α (Fig. 3).

2.3 Time Dependent Effects

Most brittle materials exhibit time dependent microcracking.⁷ This has been attributed to moisture sensitive slow crack growth in the presence of both the residual stresses and the applied stress.⁷ Time dependent strength relations based on well-established slow crack growth relations have thus been invoked to predict the influence of the stress history on the acoustic emission event rate. A typical example is the decrease in the strength s with time t at constant stress;⁷

$$s_i^{n-2} - s^{n-2} = \phi(n-2)\sigma^n t \quad (20)$$

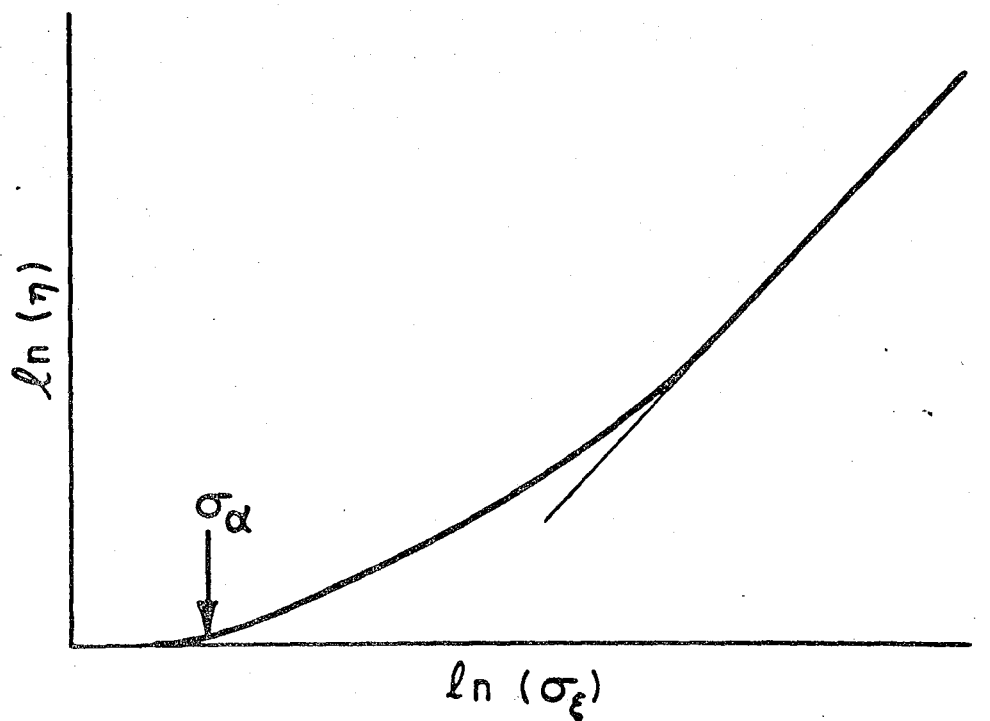
where n is a constant that reflects the propensity of the material for slow crack growth (see Eq. 33), s_i is the initial strength (at $t = 0$) and ϕ is a constant that depends on the material and the ambient moisture concentration. These time dependent strength relations can be coupled with the relation between the number of microfracture events and the strength, derived above, to yield expressions for the event rate. At constant stress σ , the total event rate $\dot{\eta}_T$ (Fig. 4) is;⁷

$$\dot{\eta}_T = \dot{\eta}_0 [1 + (m-2)\phi\sigma^2 t]^{(m-n+2)/(n-2)} \quad (21)$$

where $\dot{\eta}_0$ is the event rate at zero time. Note that, invariably $n > m+2$, so that the event rate decreases with time. The stress σ is the total stress and thus includes a thermal mismatch component and an applied stress component. Observe, however, that the thermal mismatch component is always present and the event rate associated with this stress component reduces to a negligible level soon after a temperature excursion. The initial event rate $\dot{\eta}_0$ that usually dictates the emission level is thus determined almost exclusively by the applied component of the stress (although the decay rate, with time, still depends on both components). The emission level β_0 is determined by the rate at which the load L is applied. For example, for a constant loading rate L_ℓ ;

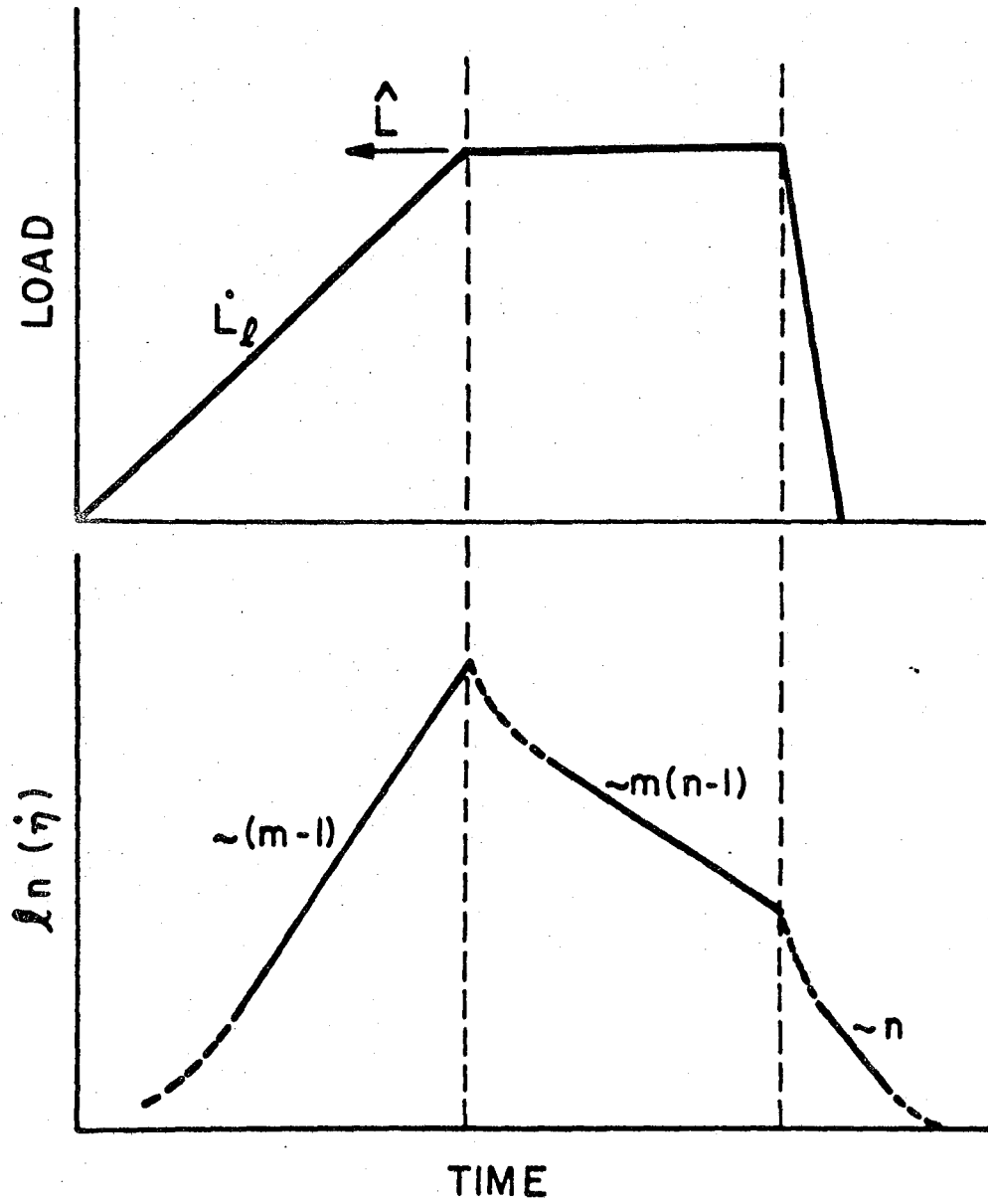
$$\dot{\eta}_T = \phi_1 \left(\frac{n-2}{n+1} \right)^{m/(n-2)} L_\ell^{[m(n-1)/(n-2)-1]} \dot{\eta}_0^{(n-m-2)/(n-2)} \quad (22)$$

where ϕ_1 is a constant. Finally, when the load is released the event rate decays rapidly with time (Fig. 4).



XBL 7811-6159

Fig. 3: A schematic indicating the dependence of the number of events η on the applied component of the stress within the inclusion, σ_ξ .



XBL7811-6158

Fig. 4: The acoustic emission event rate during a proof cycle.

One additional, and important, effect derives from the residual thermal expansion mismatch stress. The residual stress causes microcracking to proceed (in accord with Eq. (21)) when all applied stresses have been removed. The distribution of microfracture strengths thus continues to adjust to a lower level (Fig. 5); and tends toward the initial distribution, especially for a large remaining density of microcrack sites. Hence, after sufficient time has elapsed at zero load, the acoustic emission that occurs on reloading closely resembles that obtained upon initial loading, i.e., the "Kaiser effect" is virtually eliminated. This phenomenon tends to be unique to brittle materials, and has several interesting consequences (see Section 4).

III. MACROCRACK GROWTH

3.1 Stress Wave Amplitudes

The extension of a macrocrack occurs in small increments (of the order of the grain size) along the crack front (Fig. 6). For increments with relatively large extensions ℓ parallel to the crack front, the acoustic emission amplitude is closely approximated by using the displacement solution for a two dimensional crack;¹³

$$u_z = \frac{K_I}{4\mu(1+\nu)} \sqrt{\frac{r}{2\pi}} \quad (23)$$

where r is the distance from the new crack front and K_I is the opening mode applied stress intensity factor. The displacement integral over the crack surface is,

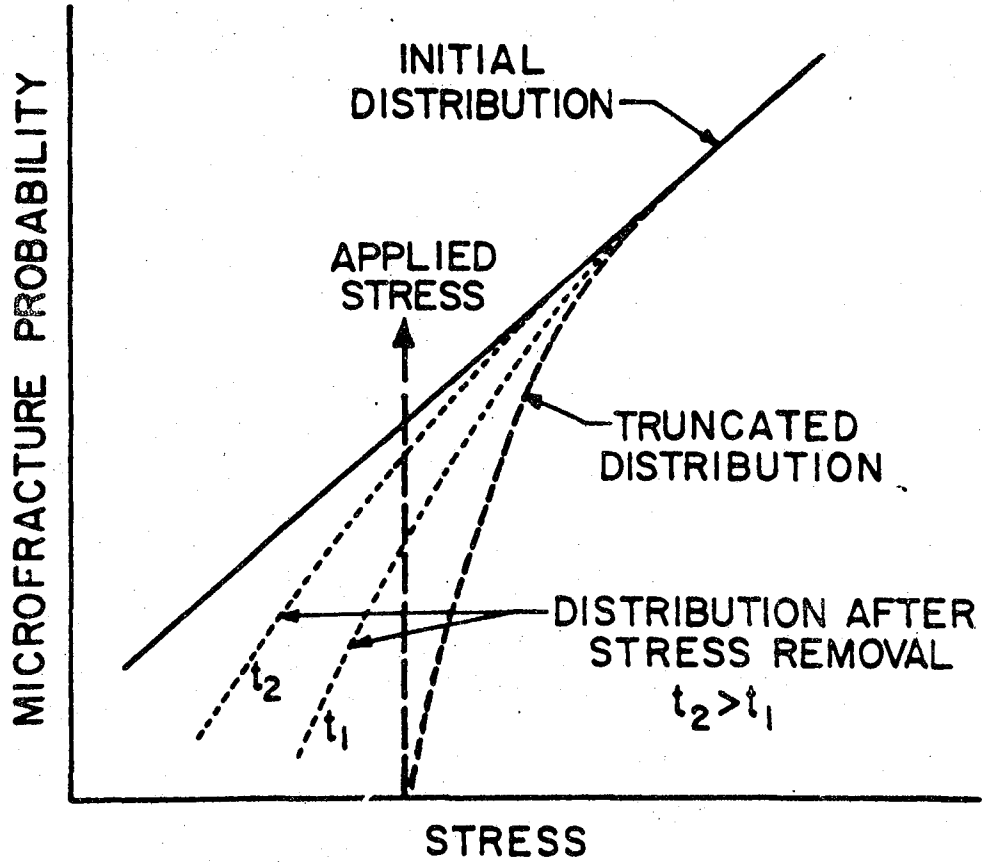
$$\begin{aligned} \int u_z dS &= \frac{K_I}{2\mu(1+\nu)\sqrt{2\pi}} \int_0^{\Delta a} \sqrt{r} dr \\ &\equiv \frac{K_I \ell (\Delta a)^{3/2}}{3\mu(1+\nu)\sqrt{2\pi}} \end{aligned} \quad (24)$$

where Δa is the crack length increment. The stress wave amplitude is thus,

$$\sigma(r,t) = \frac{K_I \ell (\Delta a)^{3/2} \delta}{3(1+\nu)\sqrt{2\pi}} \quad (25)$$

or, expressed in terms of the area ΔA swept out by the crack;

$$\sigma(r,t) = \frac{K_I \Delta A \sqrt{\Delta a} \delta}{3(1+\nu)\sqrt{2\pi}} \quad (26)$$



XBL7811-6157

Fig. 5: The effects of stress and time and the microfracture distribution function.

For crack increments in which ℓ is not large compared with Δa , the solution must be modified. Approximate upper and lower bound solutions can be obtained by assuming that the crack opening within the increment either varies as $r^{1/2}$ or is invariant. Consider the semi-circular increment, radius Δa , depicted in Fig. 6b. The upper bound displacement is

$$u_z = \frac{K_I}{4\mu(1+\nu)} \sqrt{\frac{\Delta a - x}{2\pi}} \quad (27)$$

where x is the distance from the center of the semi-circle (Fig. 6b). The displacement integral is thus;

$$\begin{aligned} \int u_z dS &\equiv \frac{\pi K_I}{4\mu(1+\nu)\sqrt{2\pi}} \int_0^{\Delta a} x\sqrt{\Delta a - x} dx \\ &= \frac{\sqrt{\pi} K_I (\Delta a)^{5/2}}{15\sqrt{2}(1+\nu)\mu} \end{aligned} \quad (28)$$

The stress wave amplitude is thus

$$\begin{aligned} \sigma(r,t) &= \frac{\sqrt{\pi} K_I (\Delta a)^{5/2}}{15\sqrt{2}(1+\nu)} \delta \\ &\equiv \frac{0.05 K_I (\Delta a)^{5/4}}{(1+\nu)} \delta \end{aligned} \quad (29)$$

The equivalent lower bound solution is;

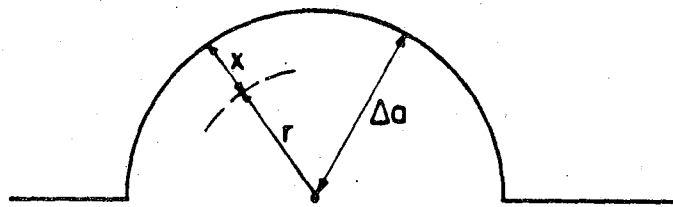
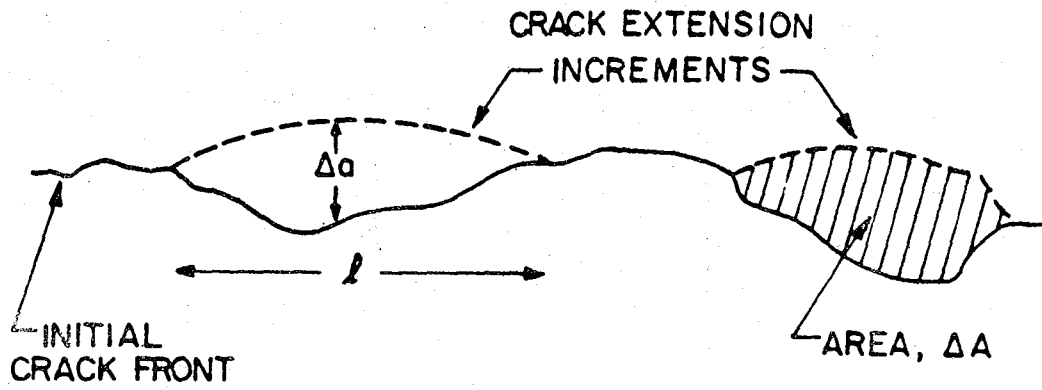
$$\sigma(r,t) = \bar{u}(K_I)\Delta a\delta \quad (30)$$

where \bar{u} is the uniform crack opening.

Examination of Eq. (26), (29) and (30) suggests a general relation for the stress wave amplitude

$$\sigma(r,t) = \delta_1 K_I (\Delta a)^q \quad (31)$$

where δ_1 is a parameter independent of the crack extension process and q is a constant in the range 1 to ~1.25.



XBL7811-6156

Fig. 6: A schematic indicating the typical mode of macrocrack extension in brittle polycrystals.

It is interesting to note that experimental studies on 7075-T6 aluminum have been interpreted to indicate an emission amplitude;

$$V = \beta_2 K_I \Delta A \quad (32)$$

where β_2 is a constant. However, since the exponent q in Eq. (31) is not expected to exceed ~ 1.25 , the experimental results are equally consistent with Eq. (31). It should be noted though that the predicted relations are only strictly applicable to fully brittle crack extension. The opening displacements are appreciably modified by crack tip plasticity, as might obtain in the aluminum alloy used to obtain the experimental results. Interestingly, however, the development of a plastic opening tends to produce a relatively uniform opening displacement and hence, as indicated by Eq. (30), q tends to unity, in close accord with the observations.

3.2 Event Rates

Finite event rates accompany macrocrack growth in materials that exhibit slow crack growth. The crack growth rate v can usually be approximated by;⁷

$$v/v_0 = (K_I/K_c)^n \quad (33)$$

where v_0 is a constant that depends on the ambient moisture content. Hence, for a sample of width b , the event rate is;

$$\dot{\eta} = \frac{bv_0}{\langle \Delta A \rangle} \left(\frac{K_I}{K_c} \right)^n \quad (34)$$

where $\langle \Delta A \rangle$ is the average area per event. The area swept out ΔA depends on the material grain size and, in some materials, on K_I . The details have been discussed previously.⁷ For the small number of brittle materials examined thus far, ΔA appears to be approximately independent of K_I , but strongly dependent on the grain size G , viz;

$$\Delta A \approx \rho G^2 \quad (35)$$

where ρ is a constant. Hence, in these materials the event rate should be a sensitive measure of K_I (or v), as generally observed. Interestingly, however, since the count amplitude also depends on K_I , a product of the event rate and the amplitude would provide an even more sensitive estimation of K_I , e.g.,

$$\dot{\eta}v = bv_0 \delta_1 (K_I^{n+1}/K_c^n) \langle \Delta A \rangle^{q-1} \quad (36)$$

Measurement parameters such as the "count rate" do include the event amplitude, but only as the logarithm; and, therefore, do not take full advantage of the amplitude effects.

IV. APPLICATIONS OF ACOUSTIC EMISSION

The acoustic emission phenomena that pertain in brittle materials have several potential applications. In materials that microcrack, the time dependence of acoustic emission can provide some indication of stress variations. Materials which exhibit appreciable sub-critical macrocrack growth, but little microcracking, are amenable to acoustic emission based failure prediction. Acoustic emission can also be used to detect and characterize transient cracking phenomena: due, for example, to thermal shock or projectile impact. Each of these applications will be briefly examined in this section.

4.1. Stress Monitoring

It has already been demonstrated that materials which microcrack can be profuse emitters of stress waves. Generally, the microcracking is found to be time-dependent (because of slow crack growth), resulting in an acoustic emission rate that depends on the details of the stress history to which the material is subject. This phenomenon can be used as a means for estimating the development of stresses in bodies which are not amenable to conventional stress analysis. The approach can be illustrated by two examples.

Porcelain is a material that is susceptible to time dependent, stress induced microcracking. Porcelain components, such as electrical insulators, are thus candidates for stress monitoring by acoustic emission. One, well-defined, example concerns the development of stresses during the proof testing of large insulators.¹⁵ The stress distribution for a fully-reversible proof test cycle can be obtained straightforwardly by finite element analysis, and the resultant acoustic emission should exhibit the characteristics depicted in Fig. 4. However, because of a metal/ceramic interface at the insulator boundaries, irreversible effects are found to occur during proof testing. The irreversibility has been attributed to lateral slippage between the insulator and the metal end caps. The magnitudes of the residual stresses that result from this irreversibility are reflected by the acoustic emission rate that develops during the unloading cycle.¹⁵

Rocks are a general class of materials that exhibit stable cracking, with both a time and a stress dependence. The stress wave emission that occurs during earth tremors should thus contain information about the stress level that produced the tremor. This phenomenon is an attractive possibility for monitoring the development of stresses in areas susceptible to earthquakes.

4.2 Failure Prediction

The dependence of the detected event rate on the stress intensity factor (Eq. 34) is the basis for the primary use of acoustic emission as a failure indicator. In principle, by measuring the event rate above a certain threshold, the average stress intensity factor can be obtained, and the remaining structural lifetime of the component may be predicted (for a known stress history).

The utility of this approach has been demonstrated for alumina¹⁶ and for zinc selenide.¹⁷ The warning period--wherein the event rate significantly exceeds the background--is only usefully large, however, at relatively low stress levels in materials that exhibit extensive slow crack growth.

The major limitation to this application of acoustic emission lies in the propensity for emission from sources other than the propagating macrocrack. These can be broadly separated into two categories: internal emission (such as microcracking or dislocation activity), or external emission (such as friction, vibration, and projectile impact). The importance of these alternate sources of emission depends on the material and the specific application. Generally, however, at least one alternate source is probable, and some method for distinguishing the emission from the macrocrack will be required. This cannot always be achieved with our present knowledge of the acoustic emission process. The alternate sources that can often be distinguished from macrofracture are; microcracking, which results in a diminishing rate of emission at constant stress (in contrast to the increasing rate from macrocrack propagation) and vibration and projectile impact, which in general only have significant emission amplitudes below ~300 kHz. The other sources, especially dislocation activity and friction, are more difficult to identify; because they do not usually have distinctively different frequency characteristics, and because event amplitude distributions and event rate relations have not yet been derived for these processes.

4.3 Transient Cracking

Cracks often develop in brittle materials during transient stress situations, such as projectile impact, abrasive wear and thermal shock. The incidence and the extent of cracking that occurs under these conditions is related to the stress waves that emanate from the cracks. Their behavior has not been analyzed, but acoustic emission can still be used as a qualitative measure of the cracking. The transient stresses that produce the fractures are an inevitable contribution to the "acoustic emission," and must be separated from the emission due to cracking. This can normally be achieved because the emission amplitudes due to impact or thermal shock decay rapidly with increase in frequency.

References

1. K. Malen and L. Bolin, Phys. Stat. Sol. 61 (1974) 637.
2. B. Budiansky and R. J. O'Connell, Intl. Jnl. Solids Structures 12, (1976) 81.
3. K. Ono, R. Landy and C. Ouchi, Proceedings of the Fourth Acoustic Emission Symposium (Tokyo, Sept. 1978).
4. E. Gumbel, Statistics of Extremes, Columbia Univ. Press: N. York (1968).
5. A. G. Evans, Acta Met., in press.
6. A. G. Evans, B. R. Tittmann, L. Ahlberg, G. S. Kino and B. T. Khuri-Yakub, Jnl. Appl. Phys. 49, (1978) 2669.
7. A. G. Evans and M. Linzer, Annual Reviews of Materials Science 7, (1977) 179.
8. Y. Nakamura, C. L. Veach and B. O. McCauley, Acoustic Emission, ASTM STP 505 p. 164.
9. A. A. Pollock, Acoustic and Vibration Progress (Ed. R.W.B. Stephens) vol. 1 (1973), p. 51.
10. A. G. Evans, B. I. Davis, G. Meyer and H. R. Baumgardner, to be published.
11. J. D. Eshelby, Proc. Roy. Soc. A241 (1957) 376.
12. J. Selsing, Jnl. Amer. Ceram. Soc. 44 (1961) 419.
13. B. R. Lawn and T. R. Wilshaw, Fracture of Brittle Solids, Cambridge Univ. Press (1975).
14. J. D. Desai and W. W. Gerberich, Engng. Frac. Mech. 7 (1973) 153.
15. A. G. Evans, S. M. Wiederhorn, M. Linzer and E. R. Fuller, Bull. Amer. Ceram. Soc. 53 (1974) 395.
16. A. G. Evans, M. Linzer and L. R. Russell, Mater. Sci. Eng. 15 (1974) 253.
17. A. G. Evans, H. Nadler, and K. Ono, Mater. Sci. Eng. 22 (1976) 7.

Figure Captions

- Fig. 1: A schematic indicating the relation between the crack opening and the emitted stress wave.
- Fig. 2: Schematics of the amplitude distribution for microcracking
(a) indicating the reduced form that applies for small Φ ;
(b) the influence of the applied stress σ^1 .
- Fig. 3: A schematic indicating the dependence of the number of events η on the applied component of the stress within the inclusion, σ_ξ .
- Fig. 4: The acoustic emission event rate during a proof cycle.
- Fig. 5: The effects of stress and time and the microfracture distribution function.
- Fig. 6: A schematic indicating the typical mode of macrocrack extension in brittle polycrystals.

This report was done with support from the Department of Energy. Any conclusions or opinions expressed in this report represent solely those of the author(s) and not necessarily those of The Regents of the University of California, the Lawrence Berkeley Laboratory or the Department of Energy.

TECHNICAL INFORMATION DEPARTMENT
LAWRENCE BERKELEY LABORATORY
UNIVERSITY OF CALIFORNIA
BERKELEY, CALIFORNIA 94720

